Nanoscale Advances

ROYAL SOCIETY OF CHEMISTRY

PAPER

View Article Online
View Journal

Cite this: DOI: 10.1039/d5na00581g

Nanoparticle-delivered miR-486-5p inhibits H_2O_2-induced injury in cultured endothelial and kidney tubular epithelial cells

Ali O. Maadelat, †[abc] Savindi Wehella, †[bc] Adrianna Douvris, [abc] Shireesha Manturthi, [bcd] Kevin D. Burns *[abc] and Suresh Gadde *[bcdef]

Acute kidney injury (AKI) is a serious condition characterized by a sudden decrease in kidney function, often leading to chronic kidney disease. Current treatment options are limited, necessitating novel therapeutic strategies. We previously showed that microRNA-486-5p (miR-486-5p) protects against AKI by regulating cell death (apoptosis) both *in vitro* and *in vivo*. However, efficient and selective delivery remains a challenge. In this study, we designed and developed nanoparticles (NPs) to encapsulate and deliver miR-486-5p to cultured endothelial and kidney tubular epithelial cells. NPs were characterized and optimized for size, polydispersity index, surface charge, and encapsulation efficiency. The stability of NPs in long-term storage and in biological solutions was confirmed. Results indicated effective cellular uptake of NPs, cargo microRNA delivery to the intracellular environment, and the absence of cytotoxicity upon NP treatment. Functional assessments showed that miR-486-5p-encapsulating lipid-polymeric hybrid NPs (HNPs) suppressed the expression of Forkhead Box Protein O1 (FOXO1), a validated target of miR-486-5p, in all cell lines investigated, suggesting effective miR-486-5p protection and transport. Both endothelial and tubular epithelial cells were significantly protected against induced apoptosis when pretreated with miR-486-5p-encapsulating HNPs. However, selective siRNA-mediated knockdown of FOXO1 did not result in injury protection, suggesting involvement of other miR-486-5p targets. Furthermore, cell injury-induced expression of inflammatory cytokines was inhibited by HNP-delivered miR-486-5p in both cell lines. These findings demonstrate the protective and anti-inflammatory effects of miR-486-5p-HNP systems in injured endothelial and tubular epithelial cells, highlighting their capacity as a potential nano-therapy for AKI and paving the way for *in vivo* studies and clinical applications.

Received 12th June 2025
Accepted 25th November 2025

DOI: 10.1039/d5na00581g

rsc.li/nanoscale-advances

1 Introduction

Acute kidney injury (AKI) is defined by an abrupt decline in kidney function.[1] It is a common complication of hospitalization and associated with increased in-hospital mortality and progressive chronic kidney disease (CKD).[1,2] One of the most prevalent causes of AKI is ischemia-reperfusion (IR) in which the blood flow to the kidneys is substantially reduced, leading to the lack of adequate oxygen (hypoxia) and nutrients necessary for cell survival.[3] Therefore, in IR cases, renal vascular endothelial cells undergo apoptosis, resulting in the irreversible rarefaction of vascular networks adjacent to tubular epithelial cells.[4] These tubular epithelial cells are responsible for the reabsorption, secretion, and regulatory functions of the kidneys. Therefore, when they experience extensive necrosis and apoptosis during IR, kidney failure occurs.[4–6] Existing clinical strategies, such as dialysis, primarily manage the consequences of AKI, such as extracellular fluid overload, uremia, and electrolyte imbalances, but no curative treatments are currently available.[2] However, in recent years, preclinical studies done by Viñas *et al.* (2016) and Douvris *et al.* (2024) have revealed that microRNA-486-5p (miR-486-5p) represents a promising therapy for AKI.[7,8]

MicroRNAs are highly conserved small non-coding RNAs (22–24 nucleotides) that regulate gene expression post-translationally.[9] Recognizing and binding target mRNAs by their seed sequence (nucleotides 2–8), microRNAs inhibit the translation of mRNAs through a variety of mechanisms, such as ribosomal hindrance and endonuclease-dependent mRNA cleavage.[9–11] In

[a]*Division of Nephrology, Department of Medicine, University of Ottawa, Ottawa, ON, Canada. E-mail: kburns@toh.ca*

[b]*Kidney Research Centre, Ottawa Hospital Research Institute, Ottawa, ON, Canada. E-mail: suresh.gadde@uottawa.ca*

[c]*Department of Cellular and Molecular Medicine, Faculty of Medicine, University of Ottawa, Ottawa, ON, Canada*

[d]*Ottawa Institute of Systems Biology, Faculty of Medicine, University of Ottawa, Ottawa, ON, Canada*

[e]*Centre for Infection, Immunity, and Inflammation, Faculty of Medicine, University of Ottawa, Ottawa, ON, Canada*

[f]*Ottawa-Carleton Institute for Biomedical Engineering (OCIBME), Ottawa, ON, Canada*

† Contributed equally.

this respect, microRNAs function similarly to small interfering RNAs (siRNAs), although there are several notable differences.[12] Most importantly, siRNAs are produced through a unique biogenesis pathway that renders them entirely complementary to their target mRNAs. Therefore, each siRNA perfectly hybridizes with and stimulates the degradation of only one mRNA, whereas microRNAs can simultaneously target multiple different mRNAs in a cell.[12]

MiR-486-5p is a muscle-enriched microRNA involved in cell survival, angiogenesis, and developmental pathways.[7,8] We have previously shown that miR-486-5p encapsulated in lipid-based carriers (lipofectamine) protects cultured human umbilical vein endothelial cells (HUVECs) exposed to hypoxia-reoxygenation by blocking apoptosis.[8,13] Furthermore, in mice and rats subjected to surgical kidney IR, tail vein injection of miR-486-5p encapsulated in lipid-based carriers reduced kidney damage markers, protected against injury, and, in rats, prevented the late development of kidney fibrosis.[7,8] While the mechanisms by which miR-486-5p functions are unclear, hundreds of genes (mRNAs) have been validated as miR-486-5p targets, such as Forkhead Box Protein O1 (FOXO1), Phosphatase and Tensin Homolog (PTEN), and Mastermind Like transcriptional Coactivator 3 (MAML3).[14,15] Despite their potential as a treatment option for AKI, there are multiple challenges in developing effective miR-486-5p-based therapeutics.[16] Notably, microRNAs are prone to rapid enzymatic degradation by nucleases, have short half-life *in vivo*, and are unable to cross the negatively charged plasma membrane to enter the cells.[17,18] Moreover, lipid-based carriers of microRNAs, such as lipofectamine and invivofectamine, have been shown to be associated *in vivo* with significant immunostimulatory, inflammatory, and off-target organ toxicity.[19–22]

Nanomedicine approaches, including nanoparticle (NP) platforms, have been incorporated into the generation of numerous RNA-based therapies.[23] NPs are sub-1000 nm size particles that can accommodate molecular cargos, such as microRNAs, in their core and protect them by their outer shell.[23,24] The latest advances in NP technology have led to the development of a variety of multifunctional NP platforms with the capacity to deliver single, dual, and multi-drug components.[24] These advances have facilitated NP tracking through imaging and selective targeting of organs, cells, and subcellular components.[25,26] Several NP-drug systems are already in clinical use, such as Onpattro and COVID-19 vaccines, or under investigation in preclinical and clinical trials.[27–31]

Due to their physicochemical properties, NP platforms have been applied in preclinical studies to various kidney disorders.[32,33] Indeed, recent studies have explored the use of NPs with diverse formulations enabling the transport of different macromolecules (*e.g.* proteins, mRNAs, siRNAs, and microRNAs) to the kidneys.[34,35] For instance, microRNA-146a packaged in polyethylenimine NPs has been shown to inhibit profibrotic and inflammatory signaling pathways in the kidneys of mice, suggesting that the delivery of appropriate microRNAs may be a therapeutic option for preventing renal fibrosis.[36] Furthermore, polymeric NPs synthesized to encapsulate and deliver microRNA-30a significantly upregulated the expression of this microRNA in glomerular podocytes of mice with diabetic nephropathy, repressing hyperglycemia-induced elevated Notch-1 signaling, enhancing podocyte survival, and reducing glomerular sclerosis.[37] However, no studies have investigated the therapeutic potential of NP-delivered microRNAs in IR-AKI. Accordingly, as an important first step toward overcoming the challenges of safe and efficient miR-486-5p delivery to ischemic-reperfused kidneys, we formulated NP platforms that encapsulate and transport miR-486-5p to endothelial and kidney tubular epithelial cells under control conditions or after oxidative stress injury.

MiR-486-5p-encapsulating NPs are designed to protect their cargo from degradation, remain stable during the treatment process, and bypass both extra- and intracellular barriers to release functional copies of miR-486-5p into the cellular cytoplasm without significant toxicity.[28,29] Additionally, for *in vivo* administration in AKI cases, NPs are designed to travel through the systemic circulation, maintain their composition, and significantly accumulate in the kidneys while resisting ongoing clearance.[38] Since the biophysical and biochemical properties of NPs directly influence their performance in each of these aspects, we designed, synthesized, characterized, and optimized four different formulations of these platforms: (1) polymeric NPs (PNPs), (2) lipid-polymeric hybrid NPs (HNPs), and (3,4) poloxamer-based NPs (Pl-NP1 and Pl-NP2). To enhance the ability of our miR-486-5p-encapsulating NPs to address AKI, we assessed their cellular uptake, stability, cytotoxicity, functionality, and impact on apoptosis using HUVECs, human proximal tubular epithelial cells (hPTECs), and human kidney tubular epithelial (HK2) cells. Our findings represent an essential step toward creating an NP-based delivery system suitable for miR-486-5p administration *in vivo* for future clinical applications.

2 Results

2.1 Nanoparticle optimization

NPs were synthesized *via* a modified nanoprecipitation method with the components shown in Fig. 1A. All NPs indiscriminately contain in their cores poly(lactic-*co*-glycolic acid) (PLGA) polymers, polyethyleneimine C14 (PEI-C14) cationic lipids, and miR-486-5p cargos stabilized through hydrophilic and electrostatic interactions. PNPs and HNPs are covered with polyethylene glycol (PEG) layers on their outermost surface to prevent aggregation and immune system detection.[39,40] Pl-NPs, on the other hand, are coated with poloxamer 188, a Food and Drug Administration (FDA)-approved biocompatible block copolymer composed of linear repeating units of poly(ethylene oxide) (PEO) and poly(propylene oxide) (PPO).[41] NPs exhibited diameters below 200 nm (Fig. 1B) and polydispersity index (PDI) values below 0.4 post-concentration (Fig. 1C), indicating that all NP solutions are relatively monodisperse. NP monodispersity was also suggested by the presence of one peak on Zetasizer intensity-size graphs (Fig. S1). The surface charges, expressed as zeta potentials, were −18.1 mV and −23.9 mV for HNP and Pl-NP2, respectively, as opposed to −4.0 mV and −4.8 mV for PNP and Pl-NP1. The efficiency of microRNA encapsulation (EE%) was between 60 and 75% for all NPs, with Pl-NP1 and Pl-

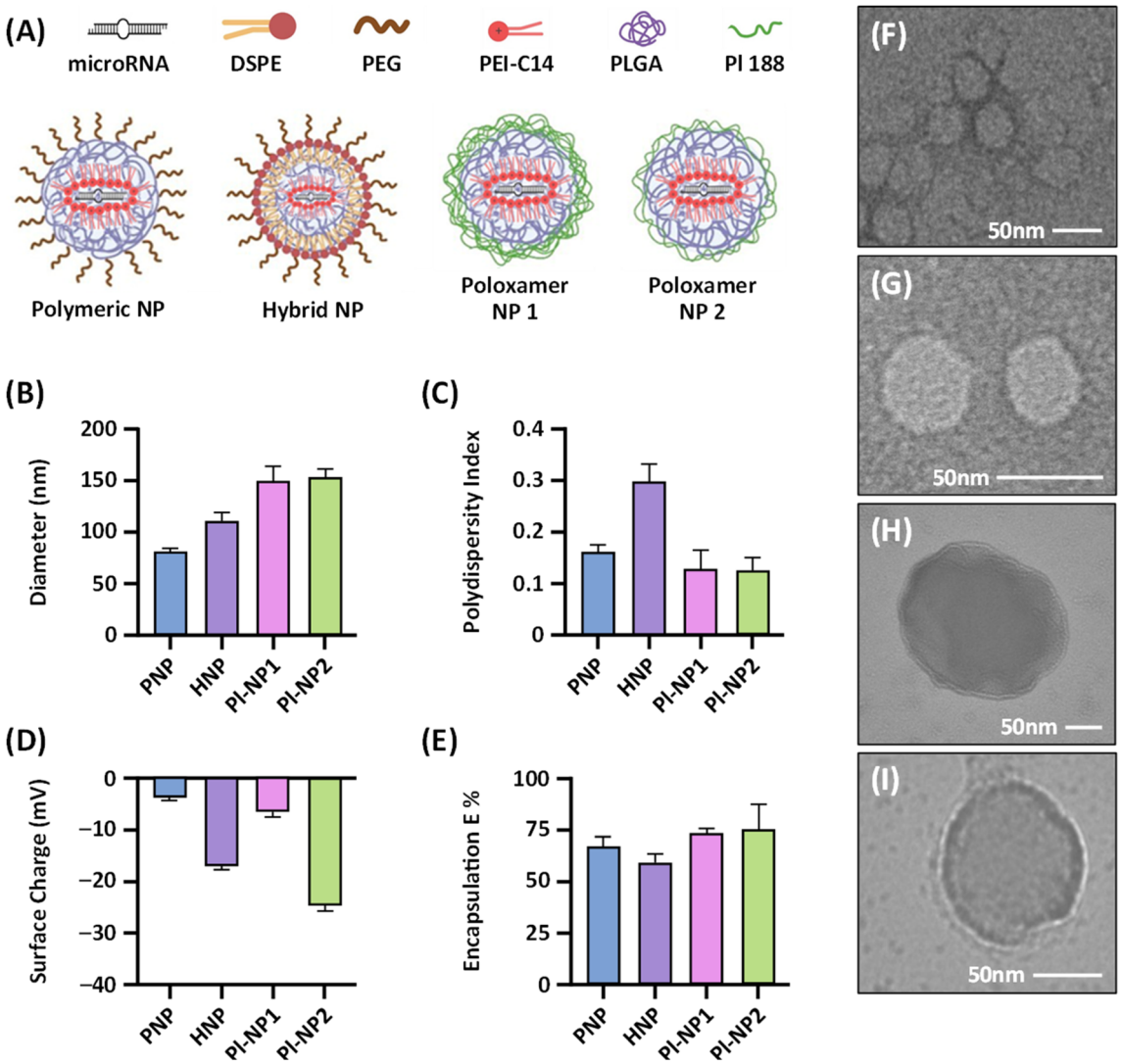

Fig. 1 Nanoparticle synthesis, characterization, and morphology. (A) Schematic representation of constituents incorporated in NP synthesis and their assumed organization. (B) Mean size (diameter; nm) of NPs encapsulating 10 nM miR-486-5p measured immediately after synthesis using a Zetasizer dynamic light scattering (DLS) instrument; $n = 5$. (C) Mean polydispersity index of NPs measured using the Zetasizer DLS instrument; $n = 3$. (D) Mean surface charge (mV) of NPs measured and expressed as zeta potentials; $n = 3$. (E) Mean encapsulation efficiency (EE%) of NPs calculated as a ratio of NP-entrapped to the total amount of 10 nM Cy5-labelled microRNA using established formulations; $n = 3$. (F) Transmission electron microscopy (TEM) image of PNPs, (G) HNPs, (H) Pl-NP1, and (I) Pl-NP2 encapsulating 10 nM miR-486-5p. Error bars represent standard error. DSPE: 1,2-distearoyl-sn-glycero-3-phosphoethanolamine. PEG: polyethylene glycol. PEI-C14: polyethyleneimine C14. PLGA: poly(lactic-co-glycolic acid). PNP: polymeric nanoparticle. HNP: hybrid nanoparticle. Pl-NP: poloxamer-based nanoparticle.

NP2 encapsulating the largest amount of cargo, followed by PNP and HNP (Fig. 1E). Lastly, transmission electron microscopy (TEM) imaging demonstrated the NPs in water post concentration with expected size and morphology (Fig. 1F).

Storage at 4 °C caused no significant alteration in the size of NPs at any time point of measurement (days 0, 15, and 30 post synthesis; Fig. 2A). To evaluate if microRNA cargos inside the NPs remained protected, RT-qPCR was performed on HUVECs 24 h post treatment with NPs that were either immediately synthesized (day 0) or synthesized and stored for 30 days at 4 °C (day 30). Although the endogenous expression of miR-486-5p in endothelial cells is negligible, we encapsulated Cel-miR-54 that is only transcribed in *Caenorhabditis elegans* inside the NPs.[7,42] As depicted in Fig. 2B, there was no significant difference between the relative Cel-miR-54 levels in HUVECs treated with day 0 *versus* day 30 NPs, indicating that NP-mediated microRNA protection and cellular uptake were unaffected after a 30 day-long storage at 4 °C. Incubation of cells with naked Cel-miR-54 resulted in no detectable increase in Cel-miR-54 levels in HUVECs.

Similarly, to ascertain the stability of NPs while they interact with proteins in biological solutions, we incubated them for 1 h at 37 °C in different concentrations of fetal bovine serum (FBS): 0%, 1%, 5%, and 10%. As shown in Fig. 2C, no significant alteration in the size of NPs was observed, suggesting NP stability.

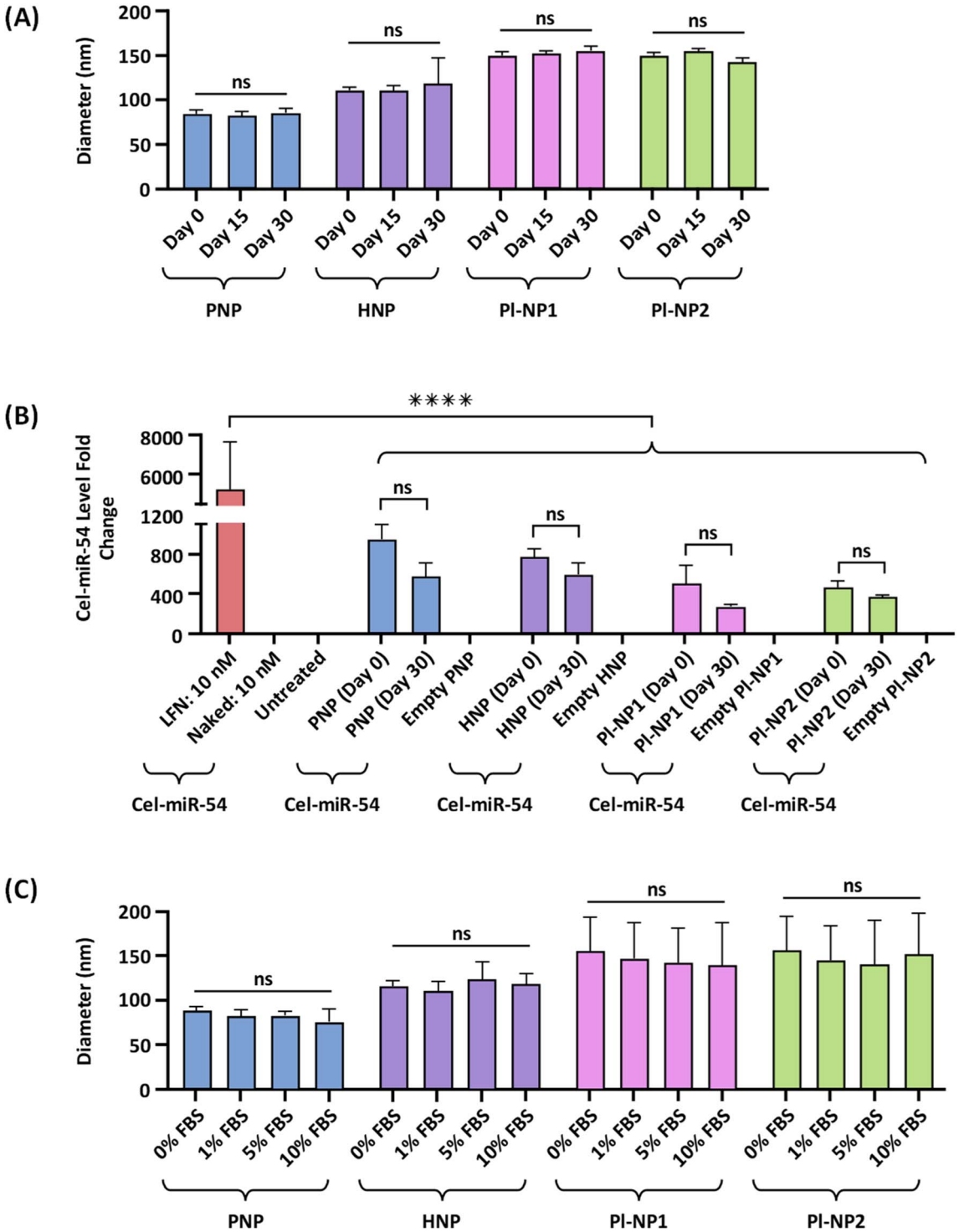

Fig. 2 Nanoparticle stability. (A) Mean size (diameter; nm) of NPs encapsulating 10 nM miR-486-5p measured using a Zetasizer dynamic light scattering (DLS) instrument after 0, 15, and 30 days of storage at 4 °C post synthesis; $n = 3$. (B) Mean fold-change in the levels of Cel-miR-54 relative to the negative control (untreated cells) measured by RT-qPCR in HUVECs 24 h post treatment with NPs encapsulating 10 nM Cel-miR-54. Lipofectamine (LFN)-borne Cel-miR-54 acted as the positive control. Naked Cel-miR-54 controlled for NP-independent delivery, which was found to be undetectable. NPs were either synthesized on the day of transfection (day 0) or 30 days earlier and stored at 4 °C (day 30); $n = 3$. (C) Mean size (diameter; nm) of NPs measured using the Zetasizer DLS instrument after 1 h of incubation in 0%, 1%, 5% and 10% fetal bovine serum (FBS) solutions at 37 °C; $n = 3$. ****$P < 0.0001$. ns = non-significant. Error bars represent standard error. PNP: polymeric nanoparticle. HNP: hybrid nanoparticle. Pl-NP: poloxamer-based nanoparticle.

2.2 Nanoparticles undergo cellular uptake and transfer microRNA

We next used Cy5-labelled microRNA (Cy5-miRs) as cargo to evaluate the NPs' ability to interact with and enter target cells. As shown in Fig. 3A, HUVECs were treated with NPs containing 10 nM Cy5-miRs and visualized after 24 h *via* fluorescent microscopy. The colocalization of cellular nuclei (blue) and the Cy5-miRs (magenta) in close proximities suggested successful cellular uptake of all four NP types, resulting in the transport of microRNA cargos inside. Furthermore, HUVECs treated with NPs containing 10 nM Cy5-miRs were subjected to flow cytometry to determine the extent of NP-cellular interaction and uptake. As demonstrated in Fig. 3B, a prominent shift was observed in the Cy5 fluorescence intensity in these cells 24 h post treatment, indicating that all NPs targeted and entered a significant portion of the cell population. These findings suggest that all NPs could interact with target cells, undergo cellular uptake, and transfer their microRNA cargos to the intracellular environment.

2.3 Nanoparticles knock down the miR-486-5p target and inhibit apoptosis with no cytotoxicity

Aiming to rescue/protect target cells from injury, NPs must cause no additional toxicity upon treatment. As shown in Fig. 4A, the lactate dehydrogenase (LDH) cytotoxicity assay revealed no significant difference in LDH levels between

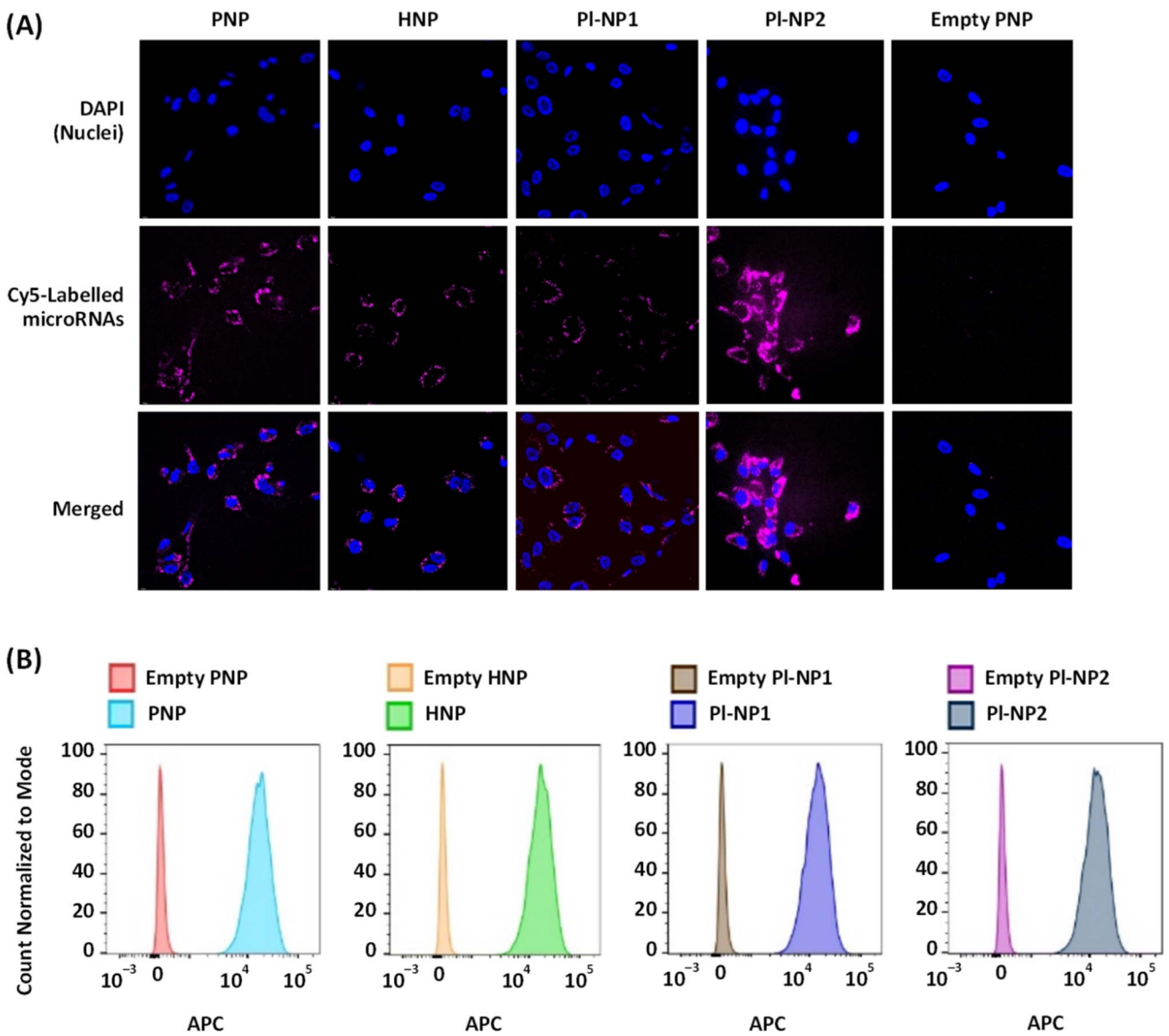

Fig. 3 Cellular uptake of nanoparticles. (A) Confocal microscopy images depicting HUVEC nuclei stained with 4′,6-diamidino-2-phenylindole (DAPI) in blue, NP-delivered Cy5-labelled microRNAs (Cy5-miRs) in magenta, and the colocalization of these fluorescent signals in the merged panels. Images were captured 24 h post treatment with NPs encapsulating 10 nM microRNA. Empty PNP treatment acted as the negative control. Magnification 100×. (B) Flow cytometry histograms depicting the count of Cy5+ HUVECs 24 h post transfection with NPs that were either empty or encapsulating 10 nM Cy5-miRs. APC: allophycocyanin. PNP: polymeric nanoparticle. HNP: hybrid nanoparticle. Pl-NP: poloxamer-based nanoparticle.

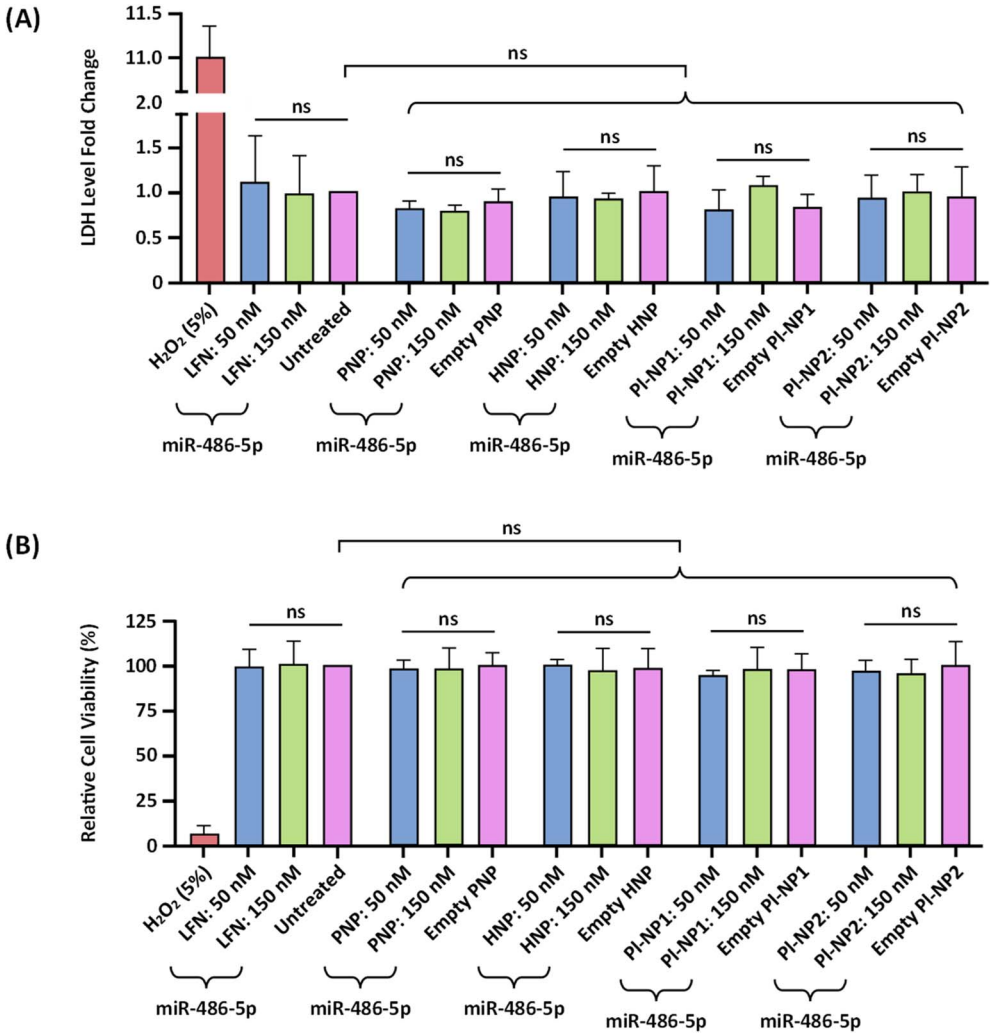

Fig. 4 Cytotoxicity and cell viability assessment of NP-encapsulated miR-486-5p. (A) Mean fold-change in lactate dehydrogenase (LDH) released into the culture medium relative to the negative control (untreated cells), measured in HUVECs 24 h post treatment with NPs that were either empty or encapsulating 50 nM or 150 nM miR-486-5p. 5% Hydrogen peroxide (H_2O_2) acted as the positive control. Lipofectamine (LFN)-borne miR-486-5p controlled for delivery efficiency; $n = 4$. (B) CCK-8 assay assessing metabolic activity by mean percent change of optical density (OD) absorbance at 450 nm relative to the negative control (untreated cells), measured in HUVECs 24 h post treatment with NPs that were either empty or encapsulating 50 nM or 150 nM miR-486-5p. 5% Hydrogen peroxide (H_2O_2) acted as the positive control. Lipofectamine (LFN)-borne miR-486-5p controlled for delivery efficiency; $n = 3$. ns = non-significant. Error bars represent standard error. PNP: polymeric nanoparticle. HNP: hybrid nanoparticle. Pl-NP: poloxamer-based nanoparticle. CCK-8: cell counting kit-8.

HUVECs treated with miR-486-5p-containing NPs (at 50 nM and 150 nM) and the untreated counterparts. Similarly, the cell counting kit-8 (CCK-8) assay (Fig. 4B) revealed no significant decrease in cell viability (metabolic activity) in HUVECs treated with miR-486-5p-containing NPs (at 50 nM and 150 nM) compared to untreated controls. These data indicate that there was no cytotoxicity associated with our miR-486-5p-NP platforms.

After successful cellular uptake, NPs must escape endosomes and release their miR-486-5p cargo into the cytosol for target mRNA translation inhibition. To evaluate the functionality of NP-delivered miR-486-5p, we measured the expression levels of FOXO1 protein, a validated mRNA target of miR-486-5p, in HUVECs and kidney tubular epithelial cells (hPTECs and HK2) 72 h post treatment with NPs containing 19.6 nM miR-486-5p.[7] As depicted in Fig. 5A and B and S2, miR-486-5p-encapsulating HNPs significantly reduced FOXO1 protein levels in all three cell lines compared to untreated cells. However, treatment of HUVECs with the other NP formulations (PNPs, Pl-NP1s, and Pl-NP2s) containing 19.6 nM miR-486-5p under similar conditions did not cause a reduction in FOXO1 protein levels (Fig. 5C). To ensure that the FOXO1 knockdown was indeed due to the activity of HNP-delivered miR-486-5p, we treated HUVECs with Cel-miR-54-encapsulating HNPs under similar conditions. As shown in Fig. 5C, no reduction in FOXO1 protein levels was evident in these cells.

Next, we evaluated the protective effect of miR-486-5p-encapsulating HNP treatment on hydrogen peroxide (H_2O_2)-induced apoptosis in HUVECs and hPTECs by measuring cleaved caspase3 (CC3) enzyme activity (schematic

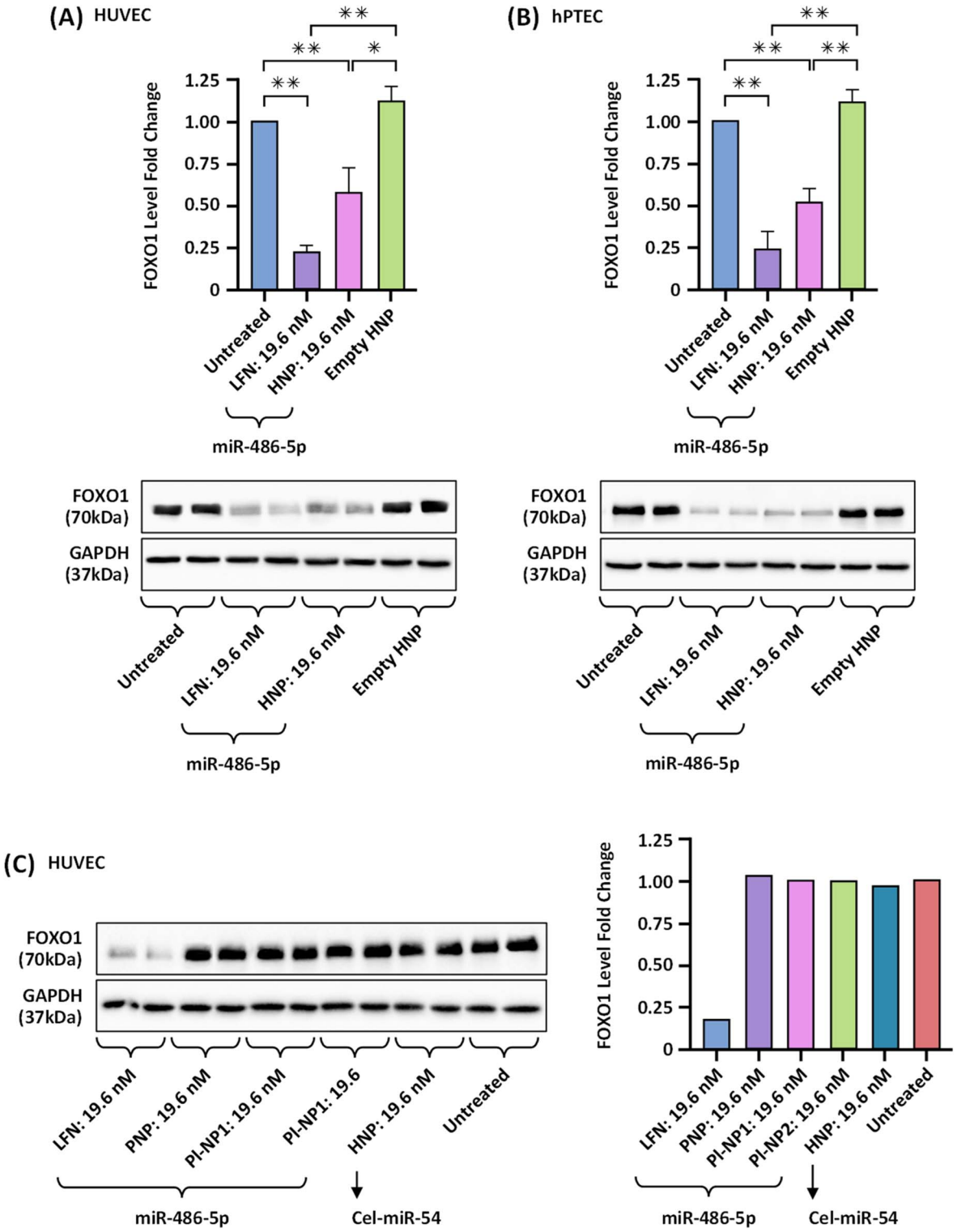

Fig. 5 Functional assessment of NP-encapsulated miR-486-5p and Cel-miR-54. (A and B) Mean levels of FOXO1 protein relative to the negative control (untreated cells) and the housekeeping GAPDH protein (loading control), measured by immunoblotting in (A) HUVECs ($n = 4$) and (B) hPTECs ($n = 3$) 72 h post treatment with HNPs that were either empty or encapsulating 19.6 nM miR-486-5p. Each pair of bands represents technical duplicates. Lipofectamine (LFN)-borne miR-486-5p acted as the positive controls. (C) Mean levels of FOXO1 protein relative to the negative control (untreated cells) and the housekeeping GAPDH protein (loading control), measured by western blotting in HUVECs ($n = 1$) 72 h post treatment with PNPs, Pl-NP1s, Pl-NP2s, and HNPs that were either empty or encapsulating 19.6 nM microRNA. PNPs, Pl-NP1s, and Pl-NP2s encapsulated miR-486-5p, and HNPs encapsulated Cel-miR-54. Each pair of bands represents technical duplicates. Lipofectamine (LFN)-borne miR-486-5p acted as the positive controls. *$P < 0.05$. **$P < 0.01$. Error bars represent standard error. FOXO1: forkhead box O1. GAPDH: glyceraldehyde-3-phosphate dehydrogenase. PNP: polymeric nanoparticle. HNP: hybrid nanoparticle. Pl-NP: poloxamer-based nanoparticle.

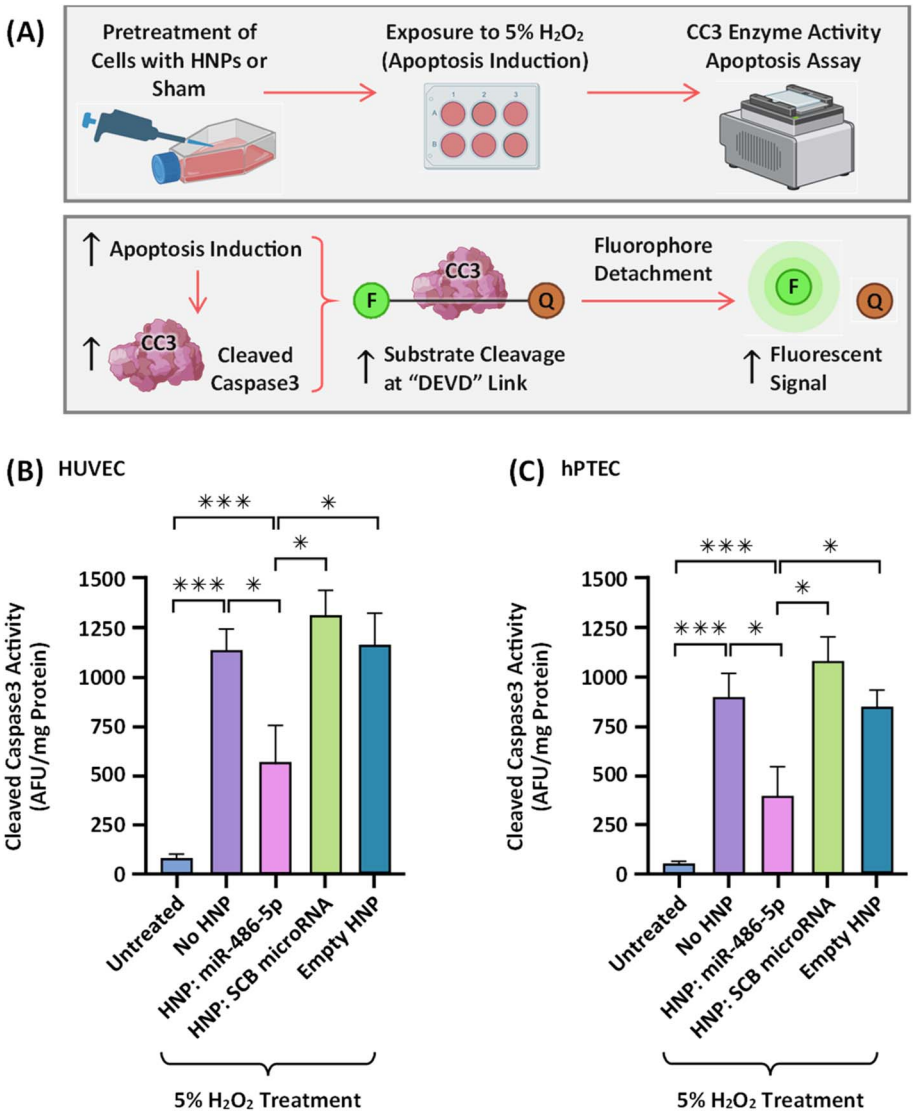

Fig. 6 Apoptosis assessment in cells treated with miR-486-5p-loaded hybrid nanoparticles (HNPs). (A) Schematic representation of cleaved caspase3 (CC3) enzyme activity assay experimental procedure with a substrate composed of a fluorophore (F) linked to a quencher (Q) by CC3 recognition sequence "DEVD." (B,C) CC3 enzyme activity assay in (B) HUVECs ($n = 5$) and (C) hPTECs ($n = 5$) treated with HNPs that were either empty or encapsulating 19.6 nM miR-486-5p or scrambled (SCB) microRNAs (negative controls) 6 h prior to 2 h of exposure to 5% hydrogen peroxide (H_2O_2). *$P < 0.05$. ***$P < 0.001$. Error bars represent standard error. HNP: hybrid nanoparticle.

representation of the assay in Fig. 6A). As depicted in Fig. 6B and C, pretreatment of HUVECs and hPTECs with miR-486-5p-encapsulating HNPs significantly inhibited apoptosis and protected the cells. This finding was also validated by preliminary flow cytometry data (Fig. S3), where measurement of annexin5 (A5) and propidium iodide (PI) signals revealed decreased apoptosis in 5% H_2O_2-exposed HUVECs and hPTECs pretreated with miR-486-5p-encapsulating HNPs.

Finally, to determine the potential role of FOXO1 targeting by miR-486-5p in the inhibition of apoptosis, and to see if independent FOXO1 knockdown could emulate miR-486-5p's protective effect, we treated cells with HNPs containing 19.6 nM FOXO1 siRNA instead of miR-486-5p under similar conditions. As shown in Fig. 7A and B, the CC3 enzyme activity assay revealed no reduction, but rather a significant stimulation, in apoptosis in HUVECs and hPTECs pretreated with FOXO1 siRNA-encapsulating HNPs prior to 5% H_2O_2 exposure. These results suggest that ubiquitous FOXO1 knockdown with siRNA, unlike miR-486-5p, does not protect the cells.

2.4 Nanoparticle-delivered miR-486-5p suppresses inflammatory cytokines

Lastly, we investigated the effects of miR-486-5p-encapsulating HNPs on H_2O_2-induced inflammation in HUVECs and hPTECs by measuring the mRNA levels of interleukin (IL)-6, tumour necrosis factor (TNF)-α, IL-4, and IL-10. As presented in Fig. 8A, H_2O_2 exposure in HUVECs markedly increased the expression of pro-inflammatory cytokines IL-6 and TNF-α, while pretreatment with miR-486-5p-encapsulating HNPs significantly inhibited TNF-α upregulation. In hPTECs, pretreatment with miR-486-5p-encapsulating HNPs attenuated the H_2O_2-triggered

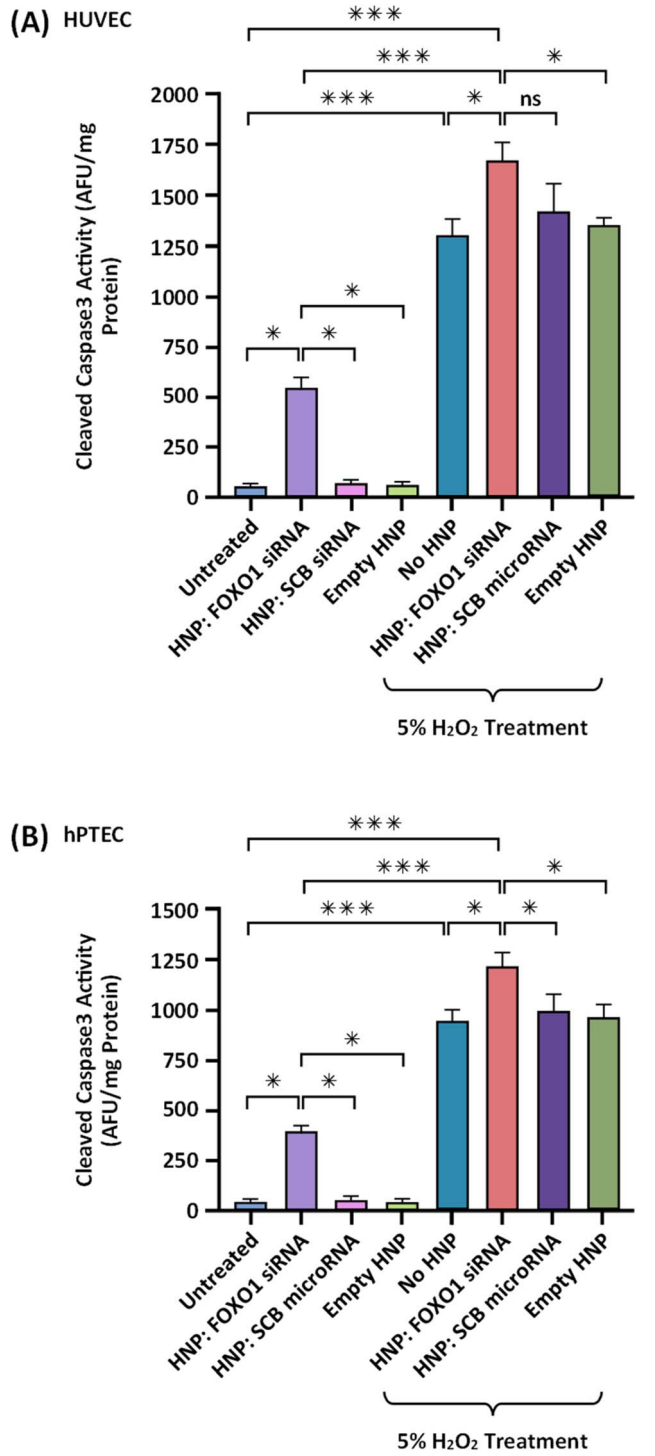

Fig. 7 Apoptosis assessment in cells treated with FOXO1 siRNA-encapsulating hybrid nanoparticles (HNPs). Cleaved caspase3 (CC3) enzyme activity assay in (A) HUVECs ($n = 3$) and (B) hPTECs ($n = 3$) treated with HNPs that were either empty or encapsulating 10 nM FOXO1 siRNA or scrambled (SCB) siRNA (negative controls) 6 h prior to 2 h of exposure to 5% hydrogen peroxide (H_2O_2) or serum-free media. *$P < 0.05$. ***$P < 0.001$. ns = non-significant. Error bars represent standard error. HNP: hybrid nanoparticle. FOXO1: forkhead box O1.

upregulation of both TNF-α and IL-6, highlighting the anti-inflammatory properties of HNP-mediated miR-486-5p delivery (Fig. 8B). The expression of anti-inflammatory cytokines IL-4 and IL-10 remained largely unaffected by the treatment of HNP-miR-486-5p systems in both cell lines.

3 Discussion

Given the severity and prevalence of AKI-related complications alongside the lack of effective treatments, novel approaches to address this condition are needed.[1,43] We have previously shown that miR-486-5p blocks IR-induced kidney injury and prevents long-term IR consequences in rodent models.[7,8,13] However, there are limitations to using microRNAs as AKI therapies since they are highly susceptible to degradation *in vivo* and cannot selectively target the kidneys.[17,44] Moreover, lipid-based carriers such as lipofectamine and invivofectamine are unsuitable for delivering miR-486-5p in clinical settings due to their high toxicity.[22] Recent studies have illustrated that these lipid-based carriers significantly damage cells at high concentrations *in vitro* and trigger adverse immune reactions *in vivo*.[19–21] To overcome these limitations, in this study we employed nanomedicine-based technologies. NPs can protect and provide for spatiotemporal delivery of a wide variety of drug macromolecules to specific organs and tissues in a vast array of diseases.[45–47] However, as the physicochemical properties of NPs directly impact their cargo encapsulation and delivery, they must be precisely optimized for their specific therapeutic purpose(s). For this reason, we developed four NP platforms to encapsulate and transport miR-486-5p into the cytosol of endothelial and kidney tubular epithelial cells.

Our NPs were synthesized using biocompatible constituents and were relatively monodisperse, encapsulating high amounts of microRNA cargo. The NPs were engineered within the size range previously shown in similar studies to be effective for renal accumulation (100–400 nm in diameter),[41,44,48,49] as evidence indicates that among various physicochemical characteristics, NP size is a major determinant of this process.[50,51] When stored at 4 °C, the NPs and their encapsulated microRNA cargos remained stable and functional for up to 30 days. Likewise, NPs maintained their integrity during incubation in biological solutions, which is essential for all *in vivo* nanotherapeutic agents. Cellular uptake assessments showed that all NPs and their microRNA cargos were internalized by the target cells 24 h post treatment. Additionally, none of the NPs caused cellular toxicity upon treatment and uptake. Next, our data in endothelial and tubular epithelial cells indicated that post treatment, HNP-delivered miR-486-5p emerged from the HNP core and inhibited FOXO1 translation. Reduction in FOXO1 protein levels is evidence for HNP's ability to protect miR-486-5p throughout the course of treatment, escape the endosomes, and release functional miR-486-5p into the cytosol for RISC binding and target mRNA recognition.[52] In contrast, treatment of miR-486-5p-encapsulating PNP, Pl-NP1, and Pl-NP2 did not decrease FOXO1 levels in the cells. Even though we did not analyze the exact mechanism of cellular internalization and endosomal escape for our NPs in the cell lines we investigated, similar NP systems have been studied using cancer cell lines.[53–56] These studies have shown that, based on NPs' properties, the cellular internalization process can be

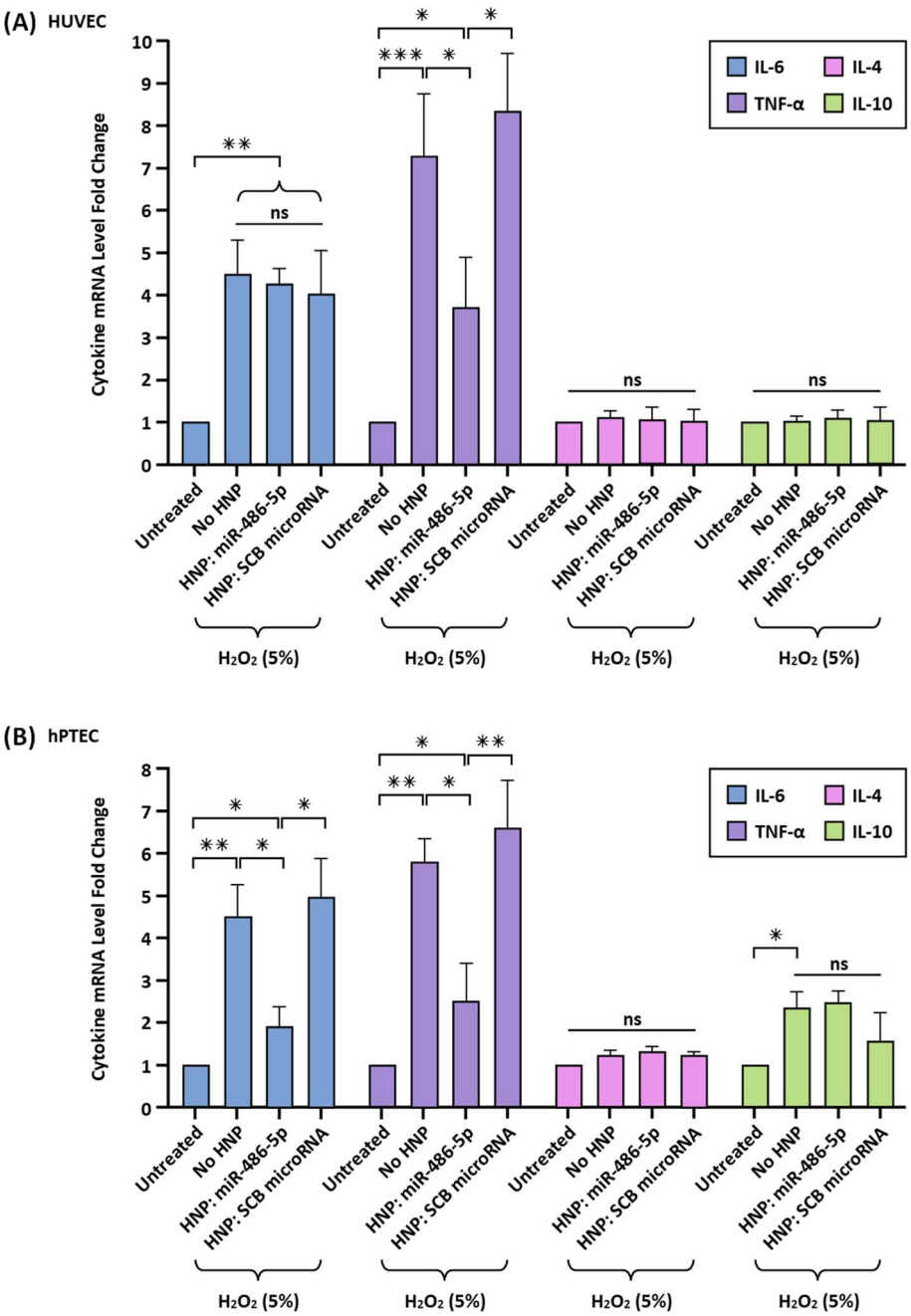

Fig. 8 Cytokine mRNA levels in cells treated with miR-486-5p-loaded hybrid nanoparticles (HNPs), with or without H_2O_2. Relative expression of IL-6, TNF-α, IL-4, and IL-10 normalized to the untreated and GAPDH housekeeping mRNA measured *via* RT-qPCR in (A) HUVECs ($n = 3$) and (B) hPTECs ($n = 3$) treated with HNPs that were encapsulating 19.6 nM miR-486-5p or scrambled (SCB) microRNAs (negative controls) 6 h prior to 4 h of exposure to 5% hydrogen peroxide (H_2O_2). *$P < 0.05$. **$P < 0.01$. ***$P < 0.001$. ns = non-significant. Error bars represent standard error. IL: interleukin. TNF-α: tumour necrosis factor-α. GAPDH: glyceraldehyde-3-phosphate dehydrogenase. RT-qPCR: real-time quantitative polymerase chain reaction.

varied from endocytic to macropinocytic pathways, and endosomal escape can be attributed to mechanisms related to membrane disruption and proton-sponge effects.[54,56–58] While the exact reason why FOXO1 was not knocked down by some of the NPs is unclear, one possibility is that these NPs might not have been able to escape cellular endosomes, or that miR-486-5p could not detach from the cationic lipids in the NP core after cellular entry.

Subsequently, apoptosis assays showed that HNP-delivered miR-486-5p significantly blocked apoptosis in cells exposed to 5% H_2O_2, suggesting that miR-486-5p-HNP systems promote cell survival by protecting against injury. Our findings also revealed that FOXO1 silencing using siRNAs did not block apoptosis in any cell line, indicating that other targets must be involved in miR-486-5p-mediated apoptosis inhibition. These targets may include (but are not limited to) PTEN, MAML3,

Forkhead Box Protein P1 (FOXP1), and Tumor Necrosis Factor Superfamily Member 4 (TNFSF4), which we have previously validated in HUVECs through RNA-sequencing of biotinylated miR-486-5p pulldown RNA.[59] Lastly, measurement of cellular cytokine mRNA levels revealed that miR-486-5p-encapsulating HNPs suppressed injury-induced inflammation by inhibiting H_2O_2-triggered upregulation of IL-6 (in tubular epithelial cells only) and TNF-α (in both endothelial and tubular epithelial cells), demonstrating that miR-486-5p is a multi-functional agent that can, through its various targets, simultaneously influence several cellular pathways.

This study has several limitations that should be acknowledged. First, all experiments were conducted *in vitro* using cultured cells that may not fully recapitulate the complexity of *in vivo* kidney injury. As such, the stability, biodistribution, renal accumulation, and therapeutic efficacy of our miR-486-5p-encapsulating NPs remain to be analyzed in animal models of IR-AKI. Second, despite their widespread use as surrogate models for renal endothelial cells, HUVECs may not be ideal representatives of the specialized endothelial populations within the kidney microvasculature.[60,61] Third, apoptosis is not the only cellular pathway that plays a role in AKI progression, and the effect of NP-delivered miR-486-5p on necrosis, pyroptosis or other autophagy processes requires further study. Lastly, while NP physicochemical properties were optimized for renal targeting in principle, their actual targeting specificity, clearance kinetics, and off-target effects *in vivo* are unknown.

Our *in vitro* findings provide an important foundation for advancing miR-486-5p-NP systems to *in vivo* evaluations. Since this stage of developing miR-486-5p-based nano-therapies for AKI focused on cultured cells, our primary method for assessing their protective effects was the measurement of cellular apoptosis. However, our next set of aims include studying the performance of miR-486-5p-encapsulating NP platforms *in vivo* using animal models with and without IR kidney injury. Further research can enhance our NP formulations and, leveraging advancements in nanotechnology, facilitate optimization of NP physicochemical characteristics (*e.g.* size) as well as specific modifications that will enable these NPs to selectively target injury-prone regions of the kidneys, such as the proximal convoluted tubules.

4 Conclusion

In summary, this study designed miR-486-5p-encapsulating NPs that target endothelial and kidney tubular epithelial cells *in vitro*. NP characterization revealed favorable qualities, no cytotoxicity, stability in biological solutions, and stability after long-term storage at 4 °C. NPs entered and transported cargo microRNAs into the intracellular environment of treated cells. HNPs containing miR-486-5p significantly knocked down the target gene FOXO1, suggesting effective miR-486-5p protection and delivery. Induced apoptosis was significantly inhibited in cells receiving miR-486-5p-HNP systems compared to the untreated cells. However, siRNA-based silencing of FOXO1 did not inhibit apoptosis, indicating likely involvement of other miR-486-5p targets in apoptosis prevention. Finally, injury-induced upregulation of inflammatory cytokines was suppressed when cells were treated with miR-486-5p-encapsulating HNPs. Given their favorable stability, functional profile, and lack of cytotoxicity, our miR-486-5p-encapsulating HNPs hold translational potential as a therapeutic platform for IR-AKI. The next steps include comprehensive preclinical *in vivo* studies to assess biodistribution, renal targeting efficiency, therapeutic efficacy, and safety, which will lay the groundwork for clinical applications.

5 Materials and methods

5.1 Materials

PLGA ester cap LG 50:50 MW: 1 kDa was obtained from Alkina Inc (Lafayette, IN USA). 1,2-distearoyl-*sn*-glycero-3-phosphoethanolamine-PEG (DSPE-PEG) 200 MW: 2805.497 and mPEG-PLGA LG 50:50 MW: 5–10 kDa were purchased from Sigma Aldrich (Oakville, ON Canada). CCK-8 assay buffer was purchased from Sigma Aldrich. PEI-C14 was chemically synthesized according to established protocols. The following reagents and kits were ordered from ThermoFisher Scientific (Waltham, MA USA): poloxamer 188 non-ionic surfactant 100X, dimethylsulfoxide (DMSO), acetonitrile (ACN), acetone, chloroform, RNAse free water, dimethylformamide (DMF), TaqMan universal master-mix II with no UNG, TaqMan microRNA reverse transcription kit (miR-486-5p primer: AM17100; Cel-miR-54 primer: 4464084), TaqMan TNF-α primer, TaqMan IL-4 primer, TaqMan IL-6 primer, TaqMan IL-10 primer, TaqMan RNA-to-CT 1-Step Kit, DAPI nuclear counterstain, and Opti-MEM Reduced Serum Medium. Lipofectamine RNAiMAX transfection reagent was obtained from Life Technologies (Carlsbad, CA USA). 0.05% Trypsin EDTA was procured from Meditech (Canton, MA USA). Fetal bovine serum (FBS) CA origin was purchased from VWR (Radnor, PA USA). miRNeasy micro kit (50) was ordered from QIAGEN (Toronto, ON Canada). The following items were purchased from American Type Culture Collection (ATCC; Boston, MA USA): HUVECs (PCS-100-013), hPTECs (PCS-400-010), HK2 cells (CRL-2190), renal epithelial cell basal medium (PCS-400-030), renal epithelial cell growth kit (PCS-400-040), and keratinocyte serum-free media bullet kit (17005-042). EBM-2 endothelial growth medium (CC-3156) and its supplemented growth factor kit (CC-4176) were ordered from Lonza (Basel-Stadt, Switzerland).

A has-miR-486 mirVana microRNA mimic (MC10546) was obtained from Ambion (Austin, TX USA). A Cy5-miR-223-3p mimic and 0.2 μmol miRIDIAN were procured from Horizon Discovery Biosciences (Cambridge, England UK). TaqMan microRNA assays which included U6 snRNA (GTGCTCGCTTCGGCAGCACATATACTAAAATTGGAACGATAC AGAGAAGATTAGCATGGCCCCTGCGCAAGGATGA-CACGCAAATTCGTGAAGCGTTCCATATTTT), hsa-miR-486-5p (UCCUGUACUGAGCUGCCCCGAG), and Cel-miR-54 (AGGAUAUGAGACGACGAGAACA) were purchased from ThermoFisher Scientific. Primary rabbit antibodies against FOXO1 (#2880) and glyceraldehyde-3-phosphate dehydrogenase (GAPDH; #2118) were ordered from Cell Signaling (Danvers, MA

USA). Goat and anti-rabbit secondary horseradish peroxidase (HRP) antibody (AB97051) was obtained from Abcam Inc. (Cambridge, England UK). Nitrocellulose membrane rolls (1620115) were procured from BioRad (Düsseldorf, Nordheim Westfalen Germany). PI, A5, and binding buffer were purchased in a Dead Cell Apoptosis Kit from ThermoFisher Scientific. Radioimmunoprecipitation assay (RIPA) buffer, CC3 assay buffer, CC3 lysis buffer, lysis solutions, and polyacrylamide gels were made according to established protocols.

5.2 Nanoparticle synthesis

Stock solutions were prepared as follows: PEI-C14 – 1 mg mL^{-1} in DMSO (PEI-C14 was derived according to established protocols and the purified compound was checked by H-NMR and ESI mass spectrometry[47]); PLGA – 5 mg mL^{-1} in acetone; PLGA-PEG – 10 mg mL^{-1} in acetone; DSPE-PEG – 2 mg mL^{-1} in sterile water; 10% and 1% poloxamer 188. Before the addition of these stock solutions to the NP synthesis vials, their respective solvents were aspirated and equal volumes of water were incorporated. In all NPs, microRNAs (25 μL, 0.05 nmol) were first mixed with PEI-C14 and after 10 min, the remaining reagents were pipetted into the synthesis vial. The solutions were stirred for 120 min on a magnetic stir plate at 300 rpm at 4 °C. The NP solutions were concentrated by centrifugation at 10×*g* for 20 min in 100 K filters (ThermoFisher Scientific).

5.3 Nanoparticle characterization

Size, PDI, and surface charge of all NPs were measured using DLS. 10 μL of the NP solution was diluted in either RNase free water or phosphate buffered saline (PBS) and transferred into a cuvette for size calculation (Zetasizer; Malvern; Vancouver, BC Canada). For TEM imaging, 20 μL of freshly generated NPs were deposited onto carbon-coated copper grids and stained, with the excess amount of the solution blotted. Once fully dried, the grids were imaged using a JEM-1400 Flash TEM (120 kv) electron microscope. To determine EE%, each NP was first loaded with 10 nM Cy5-miRs (Cy5-miR-223-3p) under dark conditions and concentrated. The NPs were then treated with DMF to release their Cy5-miR cargos. The fluorescence values were read by a BioTek microplate reader (Agilent; Santa Clara, CA USA) at 651 nm/670 nm and the amount of Cy5-miRs was estimated using a standard curve.

5.4 Cell culture

HUVECs were cultured at 37 °C in room air with 5% CO_2 in endothelial cell growth medium-2 supplemented with 2% FBS and other complementary factors (hydrocortisone, human recombinant fibroblast growth factor (hFGF), vascular endothelial growth factor (VEGF), recombinant insulin-like growth factor (R3-IGF), ascorbic acid, human recombinant epidermal growth factor (hEGF), GA-1000, heparin). hPTECs were cultured at 37 °C in room air with 5% CO_2 in renal epithelial cell basal medium supplemented with 0.5% FBS and other complementary factors (triiodothyronine, hEGF, hydrocortisone hemisuccinate, insulin, epinephrine, transferrin, and L-alanyl-L-glutamine). HK2 cells were cultured at 37 °C in room air with 5% CO_2 in keratinocyte serum-free medium supplemented with bovine pituitary extract (BPE) and hEGF. Cells were split every 2–3 days (HUVECs and HK2 cells) or 3–4 days (hPTECs) once they reached over 70% confluency. Passages 3–10 were used for all experiments.

5.5 Cellular uptake of nanoparticles

Microscopy studies were conducted with HUVECs treated with Cy5-miR (Cy5-miR-223-3p)-loaded NPs yielding a final concentration of 10 nM. The cells were seeded onto glass coverslips within 12-well plates. After 24 h of NP treatment, cells were washed with PBS and fixed in 10% formalin for 15 min, followed by 3 rounds of PBS rinsing. The slides were then incubated for 2 h with 300 nM DAPI for nuclear staining. Slides were then mounted and imaged under a confocal microscope (Thorlabs Inc., Saint-Laurent, QC Canada). Images were analyzed with ImageJ software. Flow cytometry was performed using samples treated with 20 nM Cy5-miR (Cy5-miR-223-3p)-containing NPs. After incubation at 37 °C for 24 h post treatment, the cells were trypsinized for 2 min, centrifuged at 18×*g* for 10 min, and resuspended in PBS containing 2% FBS. Gating strategies were applied to exclude debris and doublets, and positive staining was determined based on isotype control or unstained cells. The data were analyzed by FlowJo software (Tree Star Inc., Ashland, OR USA).

5.6 Total RNA extraction and RT-qPCR

Total RNA was extracted using an miRNeasy Micro Kit (QIAGEN) or TaqMan RNA-to-CT 1-Step Kit. The cells were lysed in QIAzol or wash buffer and purified following a series of centrifugation steps based on the manufacturer's protocol. Purified total RNA was eluted in RNase free water. The concentration and purity of RNA were determined with a Nanodrop2000 (ThermoFisher Scientific) by measuring the absorbance ratios at 260 nm/280 nm. Subsequently, 10 ng of total RNA was reverse transcribed with a TaqMan microRNA reverse transcription kit or TaqMan mRNA RT-qPCR primers and mastermix according to the manufacturer's protocol for miR-486-5p, Cel-miR-54, U6, TNF-α, IL-4, IL-6, IL-10, and GAPDH. Real-time qPCR was performed *via* TaqMan microRNA assay and using a TaqMan RNA-to-CT 1-Step Kit with a Bio-Rad CFX96. The expression levels of target microRNAs and mRNAs were respectively normalized to U6 and GAPDH and relative values were calculated using the ΔΔCtq method.[62]

5.7 Cytotoxicity assay

Cell viability was determined by the release of LDH into the growth medium or by metabolic activity measured *via* CCK-8 assay. In the LDH assay, HUVECs were treated with miR-486-5p-loaded NPs and 24 h post treatment, the medium was collected and centrifuged at 16 100×*g* for 15 min, the supernatant (approximately 300 μL) was isolated, and LDH in the medium was measured using a kinetic assay by the addition of PBS containing 0.02% NADH and 0.03% sodium pyruvate. Absorbances were read at 340 nm for 10 min, with readings taken at 1 min intervals. The data are presented normalized to

the negative controls. In the CCK-8 assay, HUVECs were seeded in 96-well plates at a density of 5000 cells/well, treated 24 h later with miR-486-5p-loaded NPs, and washed in CCK-8 buffer at 24 h post treatment. Optical density (OD) absorbances were read at 450 nm.

5.8 Immunoblotting

HUVECs, hPTECs, and HK2 cells were counted by a BioRad automatic counter (Mississauga, ON Canada), seeded in 6-well plates at a density of 100 000 cells/well, and treated 24 h later with NPs or lipofectamine RNAiMAX plus microRNA (10 nM or 19.6 nM). At 72 h post treatment, cells were lysed in cold RIPA buffer and centrifuged at 12 000×*g* at 4 °C for 5 min. Protein quantification was performed using the DC Protein Assay (BioRad). Lysates were then boiled, and proteins were resolved by SDS polyacrylamide gel electrophoresis, transferred to nitrocellulose membranes, blocked in 5% milk for 1 h, and incubated for 16 h at 4 °C with the primary FOXO1 antibody (1:1000). The rationale for measurement of FOXO1 levels is based on the validation of this protein as a highly prominent miR-486-5p target that is involved in multiple apoptotic and cell survival pathways.[59,63] Loading control GAPDH was incubated for 1 h at room temperature. Membranes were then incubated with horseradish peroxidase (HRP)-conjugated anti-rabbit secondary antibody (1:5000) for 1 h at room temperature and visualized by chemiluminescence (BioRad). Densitometry analyses were performed using ImageJ software (NIH; Bethesda, MD USA).

5.9 Apoptosis assessments

5% H_2O_2 was used as an *in vitro* inducer of apoptosis as it elicits oxidative stress and activates cellular pathways driven by reactive oxygen species, mimicking those observed during IR injury.[64,65]

CC3 enzyme activity was measured as previously described.[13] Briefly, HUVECs and hPTECs were lysed in cold CC3 buffer (50 mM HEPES (pH 7.4), 0.2% Triton-X, 0.15 mg mL^{-1} dithiothreitol (DTT), 0.1 mM EDTA) and centrifuged at 12 000×*g* at 4 °C for 5 min. Protein quantification was performed using the DC Protein Assay (BioRad). Cell lysates (50 μg protein/sample) were incubated at 37 °C for 16 h in the presence of a 200 μM AC-DEVD-AMC substrate (Cayman Chemicals, Ann Arbor, MI USA) with and without the AC-DEVD-CHO inhibitor (4 μM; BioMol, Farmingdale, NY USA) in assay buffer containing 50 mM HEPES (pH 7.4), 100 mM NaCl, 0.14 mg mL^{-1} DTT, 1 mM EDTA, 0.2% Trixon-X and 10% glycerol. Fluorescence was measured using a BMG FLUOstar Galaxy microplate reader (Labexchange, Burladingen, Germany) with an excitation wavelength of 360 nm and an emission wavelength of 460 nm.

For the PI-A5 flow cytometry test, post treatment with NPs, HUVECs and hPTECs were trypsinized for 2 min and centrifuged at 750×*g* at 4 °C for 10 min. The supernatant was discarded, and the cells were resuspended in 500 μL of binding buffer. 25 μL of PI and 25 μL of A5 were then mixed with the resuspension solution for 15 min under dark conditions, followed by the addition of 500 μL of binding buffer. Flow cytometry analysis was then conducted after 1 h on the FACSCalibur Flowcytometry System (BD Biosciences, New York, NY USA). The data are analyzed by FlowJo software.

5.10 Statistical analysis

All data have been presented as mean ± standard error. One-way and two-way analysis of variance (ANOVA) were used for comparisons among two and multiple groups, and *p*-values below 0.05 were considered significant. Graphs and statistical results were generated and modified using GraphPad Prism software (San Diego, CA USA), BioRender (Toronto, ON Canada), Microsoft Excel, and PowerPoint (Microsoft Office; Redmond, WA USA).

Author contributions

KDB and SG conceived, conceptualized, and co-supervised the project. SW and AOM designed and conducted experiments. AD and SM assisted in conducting some experiments. AOM drafted the initial manuscript and prepared the figures. AOM, SW, AD, SM, KDB, and SG performed data analyses and contributed to manuscript revision and editing.

Conflicts of interest

The authors report no potential conflict of interest.

Data availability

The data supporting this article have been included as part of the supplementary information (SI). Supplementary information is available. See DOI: https://doi.org/10.1039/d5na00581g.

Acknowledgements

This project was funded by grants awarded to KDB and SG from the Kidney Foundation of Canada (24KHRG-1247114) and the University of Ottawa (Translational Research Grant). It was also supported by a Natural Sciences and Engineering Research Council Discovery grant (RGPIN-2022–04398, SG) and a Canadian Institutes of Health Research Project Grant (PJT 186094, SG). The authors would like to thank the University of Ottawa Core Facility and the Ottawa Hospital Research Institute StemCore for their technical support in flow cytometry and microscopy. We also appreciate the assistance, suggestions, and comments of Dr Dylan Burger, Dr Marceline Côté, Dr Mayra T. Sonoda, Mahsa Maadelat, Angeline Thomsen, members of the G-Incs Lab, and members of the Kidney Research Centre.

References

1 J. A. Kellum, P. Romagnani, G. Ashuntantang, C. Ronco, A. Zarbock and H. J. Anders, *Nat. Rev. Dis. Primers*, 2021, 7, 52.
2 P. Pickkers, M. Darmon, E. Hoste, M. Joannidis, M. Legrand, M. Ostermann, J. R. Prowle, A. Schneider and M. Schetz, *Intensive Care Med.*, 2021, **47**, 835–850.

3 T. Kalogeris, C. P. Baines, M. Krenz and R. J. Korthuis, *Compr. Physiol.*, 2016, **7**, 113–170.
4 D. P. Basile, *Kidney Int.*, 2007, **72**, 151–156.
5 K. Makris and L. Spanou, *Clin. Biochem. Rev.*, 2016, **37**, 85–98.
6 S. Shu, Y. Wang, M. Zheng, Z. Liu, J. Cai, C. Tang and Z. Dong, *Cells*, 2019, **8**, 207.
7 A. Douvris, J. Viñas and K. D. Burns, *Cell. Mol. Life Sci.*, 2022, **79**, 376.
8 A. Douvris, J. L. Vinas, A. Gutsol, J. Zimpelmann, D. Burger and K. D. Burns, *Clin. Sci. (Lond.)*, 2024, **138**, 599–614.
9 J. O'Brien, H. Hayder, Y. Zayed and C. Peng, *Front. Endocrinol.*, 2018, **9**, 402.
10 V. Rani and R. S. Sengar, *Biotechnol. Bioeng.*, 2022, **119**, 685–692.
11 A. M. M. T. Reza and Y.-G. Yuan, *Cells*, 2021, 10.
12 J. K. Lam, M. Y. Chow, Y. Zhang and S. W. Leung, *Mol. Ther. Nucleic Acids*, 2015, **4**, e252.
13 J. L. Viñas, D. Burger, J. Zimpelmann, R. Haneef, W. Knoll, P. Campbell, A. Gutsol, A. Carter, D. S. Allan and K. D. Burns, *Kidney Int.*, 2016, **90**, 1238–1250.
14 A. Douvris, J. L. Viñas, S. Akbari, K. Tailor, M. M. Lalu, D. Burger and K. D. Burns, *Ren. Fail.*, 2024, **46**(2), 2419960.
15 J.-K. Ju, W.-N. Han and C.-L. Shi, *Bioengineered*, 2022, **13**, 4587–4597.
16 M. Y. Momin, R. R. Gaddam, M. Kravitz, A. Gupta and A. Vikram, *Cells*, 2021, 10.
17 V. Ramachandran and X. Chen, *Science*, 2008, **321**, 1490–1492.
18 C. H. Kapadia, B. Luo, M. N. Dang, N. D. Irvin-Choy, D. M. Valcourt and E. S. Day, *J. Appl. Polym. Sci.*, 2019, **137**, 48651.
19 V. Hegde, R. P. Hickerson, S. Nainamalai, P. A. Campbell, F. J. Smith, W. H. McLean and D. M. Pedrioli, *J. Contr. Release*, 2014, **196**, 355–362.
20 E. Harris, D. Zimmerman, E. Warga, A. Bamezai and J. Elmer, *Biotechnol. Bioeng.*, 2021, **118**, 1693–1706.
21 T. Wang, L. M. Larcher, L. Ma and R. N. Veedu, *Molecules*, 2018, **23**, 2564.
22 R. I. Mahato, *Adv. Drug Deliv. Rev.*, 2005, **57**, 699–712.
23 E. S. Lima, D. Dos Santos, A. L. Souza, M. E. Macedo, M. E. Bandeira, S. S. S. Junior, B. S. D. Fiuza, V. P. C. Rocha, L. M. Dos Santos Fonseca, D. D. G. Nunes, K. V. S. Hodel and B. A. S. Machado, *Pharmaceuticals (Basel)*, 2023, **16**, 1634.
24 S. Manturthi, S. El-Sahli, Y. Bo, E. Durocher, M. Kirkby, A. Popatia, K. Mediratta, R. Daniel, S.-H. Lee, U. Iqbal, M. Côté, L. Wang and S. Gadde, *ACS Nanosci. Au*, 2024, **4**, 416–425.
25 Y. Patel, S. Manturthi, S. Tiwari, E. Gahunia, A. Courtemanche, M. Gandelman, M. Côté and S. Gadde, *ACS Pharmacol. Transl. Sci.*, 2024, **7**, 3086–3095.
26 S. Gadde, *MedChemComm*, 2015, **6**, 1916–1929.
27 B. Wilson and K. M. Geetha, *J. Drug Delivery Sci. Technol.*, 2022, **74**, 103553.
28 Y. Xiao, K. Shi, Y. Qu, B. Chu and Z. Qian, *Mol. Ther., Methods Clin. Dev.*, 2019, **12**, 1–18.
29 M.-A. Nguyen, H. Wyatt, L. Susser, M. Geoffrion, A. Rasheed, A.-C. Duchez, M. L. Cottee, E. Afolayan, E. Farah, Z. Kahiel, M. Côté, S. Gadde and K. J. Rayner, *ACS Nano*, 2019, **13**, 6491–6505.
30 A. C. Anselmo and S. Mitragotri, *Bioeng. Transl. Med.*, 2019, **4**, e10143.
31 X. Huang, Y. Ma, Y. Li, F. Han and W. Lin, *Front. Bioeng. Biotechnol.*, 2021, **9**, 683247.
32 A. Roointan, R. Xu, S. Corrie, C. E. Hagemeyer and K. Alt, *J. Am. Soc. Nephrol.*, 2025, **36**, 500–518.
33 G. Sabiu, V. Kasinath, S. Jung, X. Li, G. C. Tsokos and R. Abdi, *Nephrol. Dial. Transplant.*, 2023, **38**, 1385–1396.
34 R. M. Williams, E. A. Jaimes and D. A. Heller, *Kidney Int.*, 2016, **90**, 740–745.
35 T. C. Palmer and R. W. Hunter, *Front. Cardiovasc. Med.*, 2023, **10**, 1250073.
36 Y. Morishita, T. Imai, H. Yoshizawa, M. Watanabe, K. Ishibashi, S. Muto and D. Nagata, *Int. J. Nanomed.*, 2015, **10**, 3475–3488.
37 N. Raval, P. Gondaliya, V. Tambe, K. Kalia and R. K. Tekade, *Int. J. Pharm.*, 2021, **605**, 120842.
38 A. Akinc, M. A. Maier, M. Manoharan, K. Fitzgerald, M. Jayaraman, S. Barros, S. Ansell, X. Du, M. J. Hope, T. D. Madden, B. L. Mui, S. C. Semple, Y. K. Tam, M. Ciufolini, D. Witzigmann, J. A. Kulkarni, R. van der Meel and P. R. Cullis, *Nat. Nanotechnol.*, 2019, **14**, 1084–1087.
39 N. Desai, *AAPS J.*, 2012, **14**, 282–295.
40 E. Padín-González, P. Lancaster, M. Bottini, P. Gasco, L. Tran, B. Fadeel, T. Wilkins and M. P. Monopoli, *Front. Bioeng. Biotechnol.*, 2022, **10**, 882363.
41 F. Yan, C. Zhang, Y. Zheng, L. Mei, L. Tang, C. Song, H. Sun and L. Huang, *Nanomed. Nanotechnol. Biol. Med.*, 2010, **6**, 170–178.
42 A. W. Clarke, E. Høye, A. A. Hembrom, V. M. Paynter, J. Vinther, Ł. Wyrożemski, I. Biryukova, A. Formaggioni, V. Ovchinnikov, H. Herlyn, A. Pierce, C. Wu, M. Aslanzadeh, J. Cheneby, P. Martinez, M. R. Friedländer, E. Hovig, M. Hackenberg, S. U. Umu, M. Johansen, K. J. Peterson and B. Fromm, *Nucleic Acids Res.*, 2025, **53**, D116–D128.
43 C. Tamargo, M. Hanouneh and C. E. Cervantes, *J. Clin. Med.*, 2024, **13**, 2455.
44 Y. Huang, J. Wang, K. Jiang and E. J. Chung, *J. Controlled Release*, 2021, **334**, 127–137.
45 J. Bejarano, M. Navarro-Marquez, F. Morales-Zavala, J. O. Morales, I. Garcia-Carvajal, E. Araya-Fuentes, Y. Flores, H. E. Verdejo, P. F. Castro, S. Lavandero and M. J. Kogan, *Theranostics*, 2018, **8**, 4710–4732.
46 J. Koga, T. Matoba and K. Egashira, *J. Atheroscler. Thromb.*, 2016, **23**, 757–765.
47 T. Joseph, D. Kar Mahapatra, A. Esmaeili, Ł. Piszczyk, M. Hasanin, M. Kattali, J. Haponiuk and S. Thomas, *Nanomaterials*, 2023, 13.
48 S. Brusco, G. Conte, A. Corteggio, T. Silvestri, A. Spitaleri, P. Brocca, A. Miro, F. Quaglia, I. d'Angelo, L. D'Apice,

P. Italiani, G. Costabile and F. Ungaro, *Adv. Healthcare Mater.*, 2024, **13**, e2402688.
49 E. L. Vallorz, J. Janda, H. M. Mansour and R. G. Schnellmann, *Kidney Int.*, 2022, **102**, 1073–1089.
50 C. H. Choi, J. E. Zuckerman, P. Webster and M. E. Davis, *Proc. Natl. Acad. Sci. U. S. A.*, 2011, **108**, 6656–6661.
51 R. M. Williams, J. Shah, H. S. Tian, X. Chen, F. Geissmann, E. A. Jaimes and D. A. Heller, *Hypertension*, 2018, **71**, 87–94.
52 A. K. L. Leung, *Trends Cell Biol.*, 2015, **25**, 601–610.
53 X. Zhu, Y. Xu, L. M. Solis, W. Tao, L. Wang, C. Behrens, X. Xu, L. Zhao, D. Liu, J. Wu, N. Zhang, I. I. Wistuba, O. C. Farokhzad, B. R. Zetter and J. Shi, *Proc. Natl. Acad. Sci. U. S. A.*, 2015, **112**, 7779–7784.
54 M. A. Islam, J. Y. Shin, J. Firdous, T. E. Park, Y. J. Choi, M. H. Cho, C. H. Yun and C. S. Cho, *Biomaterials*, 2012, **33**, 8868–8880.
55 M. A. Islam, C. H. Yun, Y. J. Choi, J. Y. Shin, R. Arote, H. L. Jiang, S. K. Kang, J. W. Nah, I. K. Park, M. H. Cho and C. S. Cho, *Biomaterials*, 2011, **32**, 9908–9924.
56 S. Chatterjee, E. Kon, P. Sharma and D. Peer, *Proc. Natl. Acad. Sci. U. S. A.*, 2024, **121**, e2307800120.
57 M. A. Islam, Y. Xu, W. Tao, J. M. Ubellacker, M. Lim, D. Aum, G. Y. Lee, K. Zhou, H. Zope, M. Yu, W. Cao, J. T. Oswald, M. Dinarvand, M. Mahmoudi, R. Langer, P. W. Kantoff, O. C. Farokhzad, B. R. Zetter and J. Shi, *Nat. Biomed. Eng.*, 2018, **2**, 850–864.
58 P. Paramasivam, C. Franke, M. Stoter, A. Hoijer, S. Bartesaghi, A. Sabirsh, L. Lindfors, M. Y. Arteta, A. Dahlen, A. Bak, S. Andersson, Y. Kalaidzidis, M. Bickle and M. Zerial, *J. Cell Biol.*, 2022, **221**, e202110137.
59 A. Douvris, A. Maadelat, C. J. Porter, D. Burger and K. D. Burns, *J. Cell. Mol. Med.*, 2025, **29**, e70589.
60 J. L. Vinas, M. Spence, C. J. Porter, A. Douvris, A. Gutsol, J. A. Zimpelmann, P. A. Campbell and K. D. Burns, *Kidney Int.*, 2021, **100**, 597–612.
61 K. Zhang, R. Li, X. Chen, H. Yan, H. Li, X. Zhao, H. Huang, S. Chen, Y. Liu, K. Wang, Z. Han, Z. C. Han, D. Kong, X. M. Chen and Z. Li, *Adv. Sci. (Weinh.)*, 2023, **10**, e2204626.
62 K. J. Livak and T. D. Schmittgen, *Methods*, 2001, **25**, 402–408.
63 X. Zhang, N. Tang, T. J. Hadden and A. K. Rishi, *Biochim. Biophys. Acta*, 2011, **1813**, 1978–1986.
64 O. Baraldi, F. Bianchi, V. Menghi, A. Angeletti, A. L. Croci Chiocchini, M. Cappuccilli, V. Aiello, G. Comai and G. La Manna, *J. Inflamm. Res.*, 2017, **10**, 135–142.
65 A. K. Salahudeen, E. C. Clark and K. A. Nath, *J. Clin. Invest.*, 1991, **88**, 1886–1893.